Journal of Visualization, Vol. 12, No. 3 (2009) 233-240

Regular Paper

Global Visualization and Quantification of Compressible Vortex Loops

Zare-Behtash, H.,* Gongora-Orozco, N. * and Kontis, K.*

* The University of Manchester, School of MACE, George Begg Building, Manchester M60 1QD, UK.
E-mail: k.kontis@manchester.ac.uk

Received 14 March 2008
Revised 18 December 2008

Abstract: The physics of compressible vortex loops generated due to the rolling up of the shear layer upon the diffraction of a shock wave from a shock tube is far from being understood, especially when shock-vortex interactions are involved. This is mainly due to the lack of global quantitative data available which characterizes the flow. The present study involves the usage of the PIV technique to characterize the velocity and vorticity of compressible vortex loops formed at incident shock Mach numbers of $M=1.54$ and 1.66. Another perk of the PIV technique over purely qualitative methods, which has been demonstrated in the current study, is that at the same time the results also provide a clear image of the various flow features. Techniques such as schlieren and shadowgraph rely on density gradients present in the flow and fail to capture regions of the flow influenced by the primary flow structure which would have relatively lower pressure and density. Various vortex loops, namely, square, elliptic and circular, were generated using different shape adaptors fitted to the end of the shock tube. The formation of a coaxial vortex loop with opposite circulation along with the generation of a third stronger vortex loop ahead of the primary with same circulation direction are of the interesting findings of the current study.

Keywords: PIV, Shock Tube, Compressible Vortex Loop, Secondary Vortex Loop.

1. Introduction

Non-circular jets provide efficient passive flow control at relatively low cost since they rely solely on changes in the geometry of the nozzle. The applications include improved large and small scale mixing, enhanced combustor performance, noise suppression, heat transfer, and thrust vector control (Gutmark and Grinstein, 1999). Non-circular injectors such as elliptic, triangular, and square nozzles are used to improve combustion processes by augmenting heat release, reducing emissions, and improving flame stability. Combustion systems with triangular and square jets (i.e., with corners) benefit from the combination of small- and large-scale mixing. The large-scale vortices promote fast bulk mixing between fuel and air, while small-scale turbulence accelerates the combustion rate by enhancing mixing at the molecular level.

Investigation into the properties of non-circular jets has been motivated by their enhanced characteristic entrainment properties relative to those of comparable circular jets. This enhanced entrainment is believed to be mainly the result of self-induced vortex ring deformations. Increased mixing of the jet plume with the surroundings which decreases jet detection is a key goal in the design of stealth aircraft.

Although numerous authors have studied both experimentally and numerically the behavior of incompressible vortex rings (Dhanak and DeBernardinis, 1981, Oshima et al., 1988, Grinstein and DeVore, 1996, Yoon and Lee, 2003), relatively speaking, not much work covering the compressible and detonation regime has been done. At high Mach numbers the flow becomes much more complicated due to the presence of shock waves within the flow. Another feature which is not uncommon (see the work of Kontis et al., 2006) is the formation of a secondary vortex loop ahead of the primary vortex loop. The following study applies the PIV technique to a shock tube with various exit geometries to generate compressible vortex loops of various geometries and focuses on this particular element of the flow, namely, the secondary vortex loop examining the formation and behavior of this particular element of the flow.

Because the main focus is on the vortex loop itself, the disturbances arising from having different driver pressures had to be eliminated by using the critical driver length for each diaphragm pressure ratio. These disturbances are formed as a result of the rarefaction waves which reflect from the closed end of the shock tube. In order to better compare the vortex loop behavior at various Mach numbers, it is desirable to eliminate these distortions. A means of doing so is by changing the length of the driver section so that the incident shock and the initial reflected rarefaction wave arrive at the shock tube exit at approximately the same time (Kontis et al., 2008, Arakeri et al., 2004, Brouillette and Hebert, 1997).

2. Setup

2.1 Shock Tube

Experiments have been carried out using air as both the driver and driven gas with diaphragm pressure ratios $P_4/P_1 = 8$ *and* 12. Where P_4 is the pressure within the driving compartment of the shock tube and P_1 is the pressure inside the driven section. From 1-D shock tube theory the aforementioned diaphragm pressure ratios correspond to incident Mach numbers of approximately $M=1.54$ and 1.66, respectively. An industrial film diaphragm has been used to divide the two sections of the shock tube. The thickness of the diaphragm was chosen to be $55\mu m$ and $75\mu m$. The bursting of the diaphragm was initiated manually with a plunger. The shock tube setup was identical to that used by Kontis et al. (2008).

Various adaptors were designed that could be attached to the end of the shock tube so that vortex loops of different shapes could be studied, as shown in Fig. 1. These include a square nozzle with side lengths of $30mm$, two elliptical nozzles with minor to major axes ratios of 0.6 and 0.4 and finally a small circular nozzle with an internal diameter of $15mm$. All the nozzles had a wall thickness of $4mm$ similar to the main shock tube.

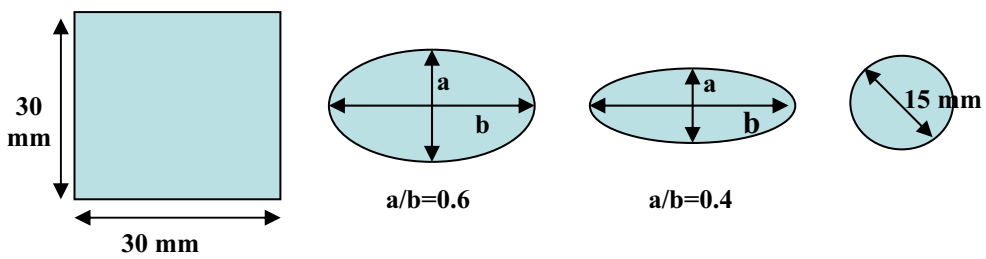

Fig. 1. Geometry of the nozzles used in the current study.

2.2 PIV Setup

Particle Image Velocimetry is based on the measurement of the velocity of tracer particles carried by the fluid (Raffel et al., 1998). Figure 2 shows the schematic of the experimental setup used. For the current study, a high frame rate PIV system consisting of a high repetition rate laser ($10m$J at $1kHz$)

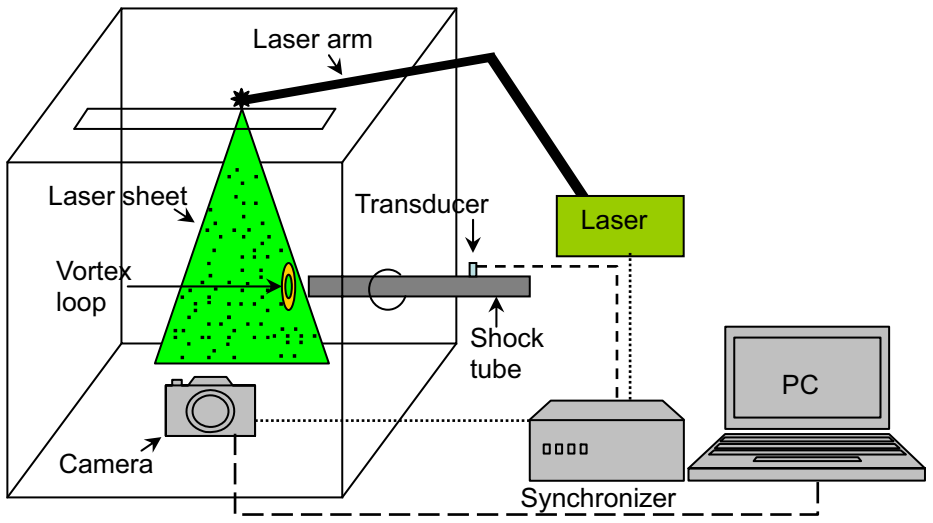

Fig. 2. Schematic of the experimental setup.

for illumination, with a light arm for easy manipulation of the laser beam and a range of light sheet optics, was used. A high frame rate Photron APX RS camera with *1024×1024* pixels resolution at *1500* frames per second and pixel size of *17μm ×17μm* was used to capture data in an on board memory of 8GB.

A *TSI* model *9306A* six-jet atomizer was used to generate seeder particles of approximately *4μm* in size. A synchronizer allows control of timing of capture and has the facility for external inputs for triggering the PIV system. A high specification PC with *TSI*s Insight PIV software installed enables data download and data analysis. The software provided includes many PIV and PTV (particle tracking velocimetry) algorithms. In addition TecPlot 10 is also loaded for data display and analysis (with TSI Plot PIV add on). The time between the two laser pulses $\Delta T = 3\mu s$ with interrogation zones of *32×32* pixels.

A transducer placed along the shock tube (shown in Fig. 2) was used to trigger image acquisition. The pressure pulse generated by the passage of the shock wave acted as the trigger. The arrival of the shock wave at this location was taken as the t=0 for the experiments. Using an external delay generator the triggering of the laser could be delayed and a sequence of images was captured.

An enclosure was designed which encased the exit of the shock tube. Prior to each run, this enclosure was filled with tracer particles along with the driven section of the shock tube so that each time the shock tube was fired the flow would discharge into the chamber which was filled with tracer particles allowing for the better study of the fluid entrainment properties of the vortex loops. The repeatability error was 1.5% for all PIV measurements.

3. Results and Discussions

At the Mach numbers studied, *M=1.54* and *1.66,* a secondary vortex loop appears ahead of the main vortex loop. The formation of this secondary vortex loop is accompanied by the decreases in axial velocity of the flow tending to flatten the protruding flow front. In some cases a third, stronger and larger vortex loop compared to the secondary vortex loop of opposite circulation is formed ahead of the main loop.

3.1 Square Vortex Loop

Figure 3 shows the velocity and vorticity contours along with the flow streamlines for the square nozzle at *M=1.54*. The yellow dashed box of Fig. 3(a) shows the observation area used for data processing. We can see the protruding flow front is quite convex with the maximum velocity occurring between the two oppositely rotating cores (Fig. 3(b)). The shear layer following the ejection of the main vortex loop is also evident in Fig. 3(c). At later times, a secondary counter-rotating vortex

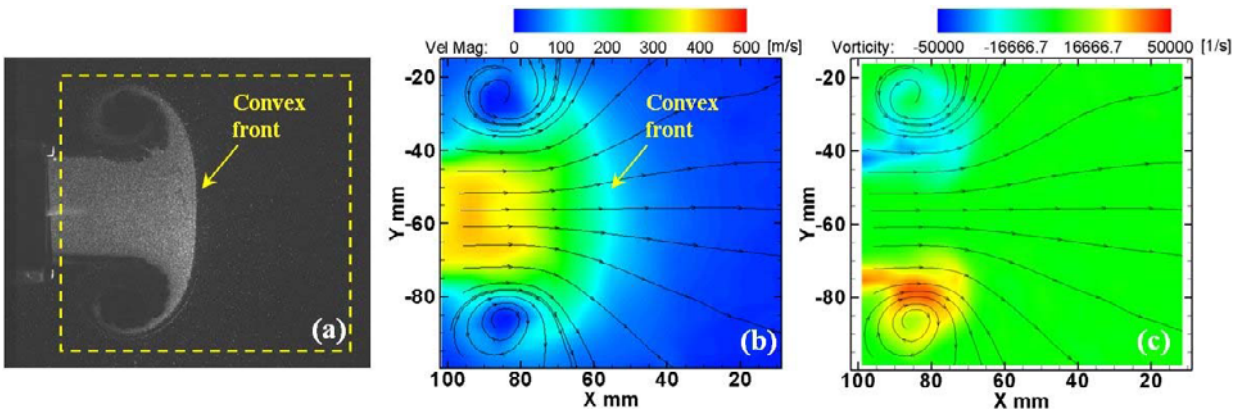

Fig. 3. Square nozzle, *M=1.54*, *t=1.22ms*, (a) raw image, (b) velocity contour, (c) vorticity contour

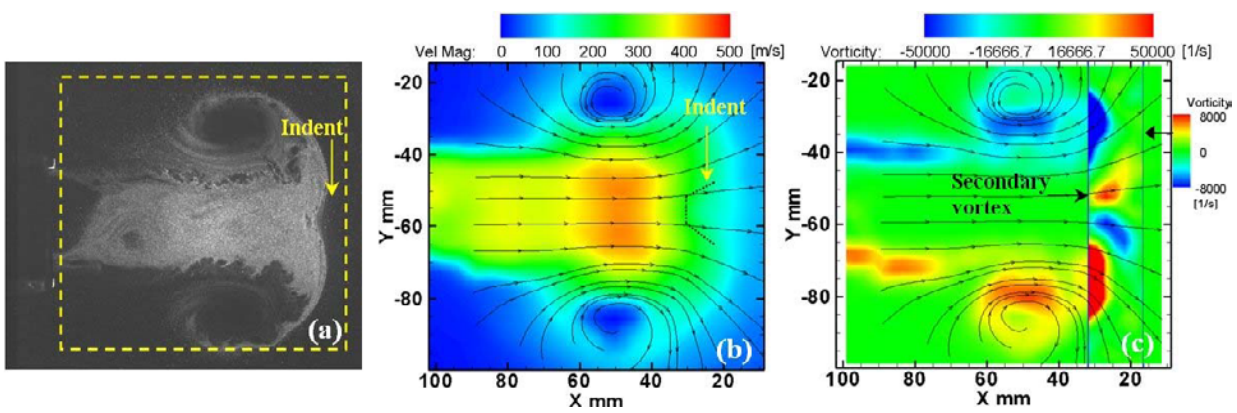

Fig. 4. Square nozzle, *M=1.54*, *t=1.47ms*, (a) raw image, (b) velocity contour, (c) vorticity contour

loop forms ahead of the main loop decreasing the velocity at the front, which is the reason for the flattening and also the slight indentation of the original convex shape and the velocity distribution of the flow field (Fig. 4(a) and 4(b)). The vorticity profile of Fig. 4(c) has been adjusted such that the secondary vortex loop is easier to discern.

At a higher Mach of *M=1.66*, as shown in Fig. 5, the flattening of the flow frontier is more pronounced as are the disturbances present in the shear layer between the two vortex cores. In Fig. 5(b) the flow exiting the tube exhibits a quite uniform velocity distribution across its span. Similar to the lower Mach number case (Fig. 4) there is a small coaxial vortex loop with opposite circulation present ahead of the main vortex loop which is believed to be responsible for the deceleration of the flow frontier leading to the indented front visible in the velocity contour of Fig. 5(b). In Fig. 5(c) the scale has been drastically reduced in order to make the secondary vortex clearer. Here we can clearly see its opposite circulatory motion.

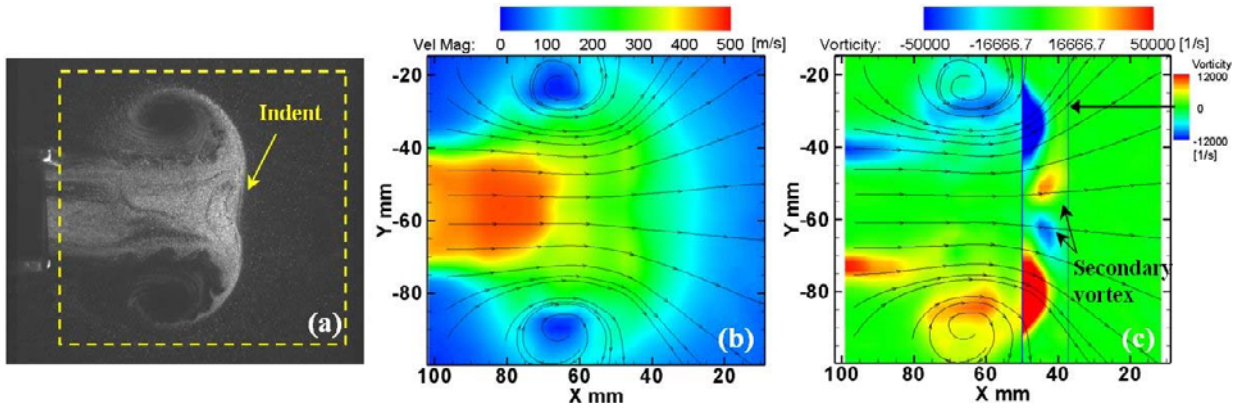

Fig. 5. Square nozzle, *M=1.66*, *t=1.12ms*, (a) raw image, (b) velocity contour, (c) vorticity contour

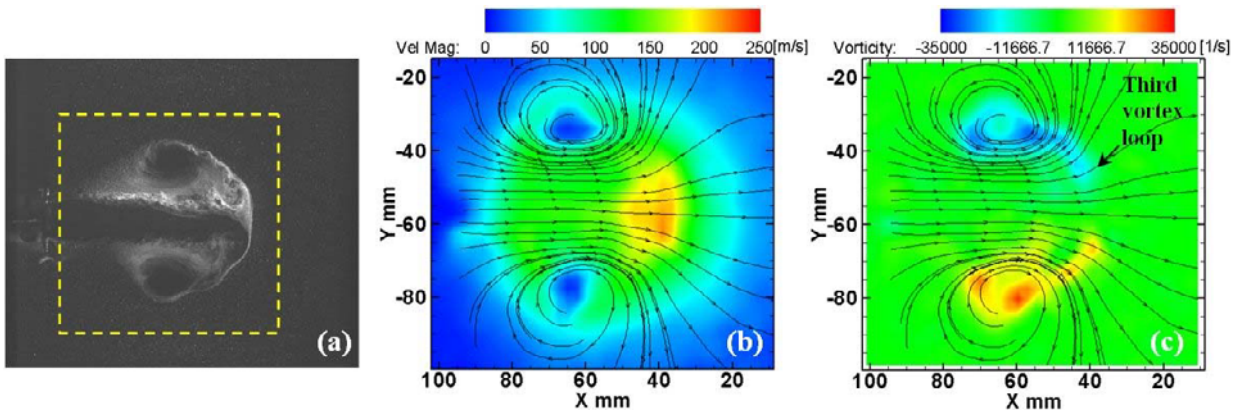

Fig. 6. Elliptic nozzle *0.4*, *M=1.54*, *t=1.22ms*, (a) raw image, (b) velocity contour, (c) vorticity contour

A diaphragm shock which is present between the two main cores in Fig. 5(b) is responsible for the decelerating of the high speed flow at the location of the two primary vortex cores.

3.2 Elliptic Vortex Loop 0.4

The vortex loop generated from the elliptic nozzle with axes ratio of *0.4* at *M=1.54*, shown in Fig. 6, has a behavior different from the square vortex loop. Firstly, the deceleration of the flow caused by the formation of the secondary vortex is less pronounced (at the instance of Fig 6 for *t=1.22ms* the secondary counter-rotating vortex loop has dissipated and is not visible in the figure). Secondly, a third vortex loop with same circulation direction as the main loop is formed ahead of it (Fig 6(c)). This third vortex loop is stronger and larger than the secondary one. The formation of this vortex loop is accompanied by an acceleration of the flow ahead of the main vortex loop (Fig. 6(b)). The acceleration of the flow which acts as a pulse could be the main reason for the generation of this third vortex loop which diminishes the secondary one. The same flow behavior was noted for *M=1.66*.

3.3 Elliptic Vortex Loop 0.6

For the elliptic nozzle with minor to major axis ratio of *0.6*, similar to the smaller elliptic nozzle the velocity of the flow is greatest at the perimeter between the two primary cores and the secondary vortex loop was formed as well as the third vortex loop visible in Fig 7(c) for a flow Mach number *M=1.54*. The instability vortices present in the shear layer are more pronounced for the larger elliptic vortex loop. In Fig. 7(b) we also observe the process of vortex pinching, which is a common feature of incompressible vortex loops. During this phase the primary vortex loop separates from the fluid emerging from the tube and propagates under its own strength. This is indicated by the reduction in speed of the flow between the main vortex loop and the shock tube exit. The streamlines of Fig. 7(b) and 7(c) show the circulation of the main vortex cores influencing a region approximately *40mm*

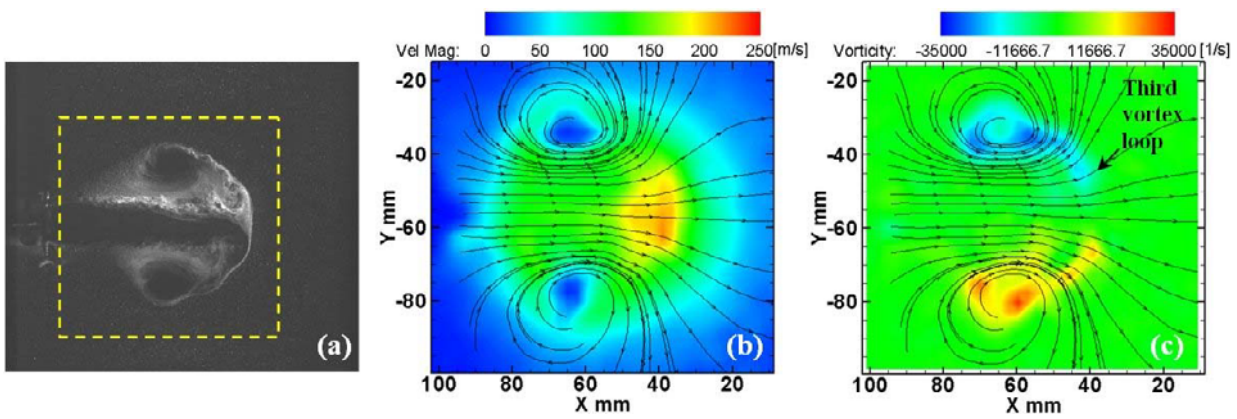

Fig. 7. Elliptic nozzle *0.6*, *M=1.54*, *t=1.26ms*, (a) raw image, (b) velocity contour, (c) vorticity contour

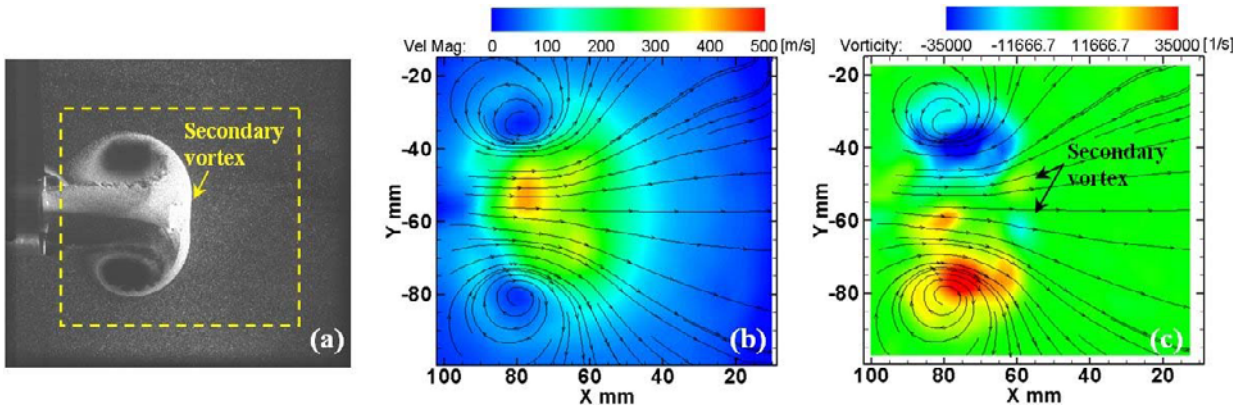

Fig. 8. Elliptic nozzle *0.6*, *M=1.66*, *t=0.97ms*, (a) raw image, (b) velocity contour, (c) vorticity contour

ahead of the main cores.

At a higher Mach number of *M=1.66*, the secondary vortex becomes stronger as shown in Fig 8(c). The velocity contour in Fig. 8(b) shows an increased velocity of the flow at the location of the secondary vortex loop. The formation of the secondary vortex is induced by the motion of the primary vortex. At higher Mach numbers since the vorticity of the main vortex is higher, the opposite circulation induced on the flow ahead of it is also greater. At later times third vortex loop noted for the smaller elliptic vortex loop visible in Fig. 8(c) was also noted.

3.4 Circular Vortex Loop 15mm

The small circular nozzle behaves in a completely unique way. Although it initially starts out as a conventional circular vortex loop it quickly goes through a morphological transformation. Figs. 9 and

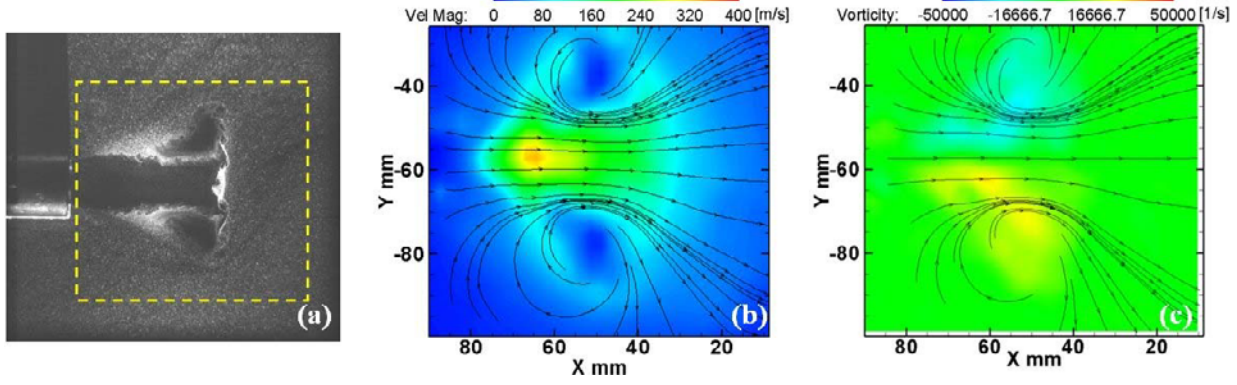

Fig. 9. Circular nozzle, *M=1.54*, *t=1.16ms*, (a) raw image, (b) velocity contour, (c) vorticity contour

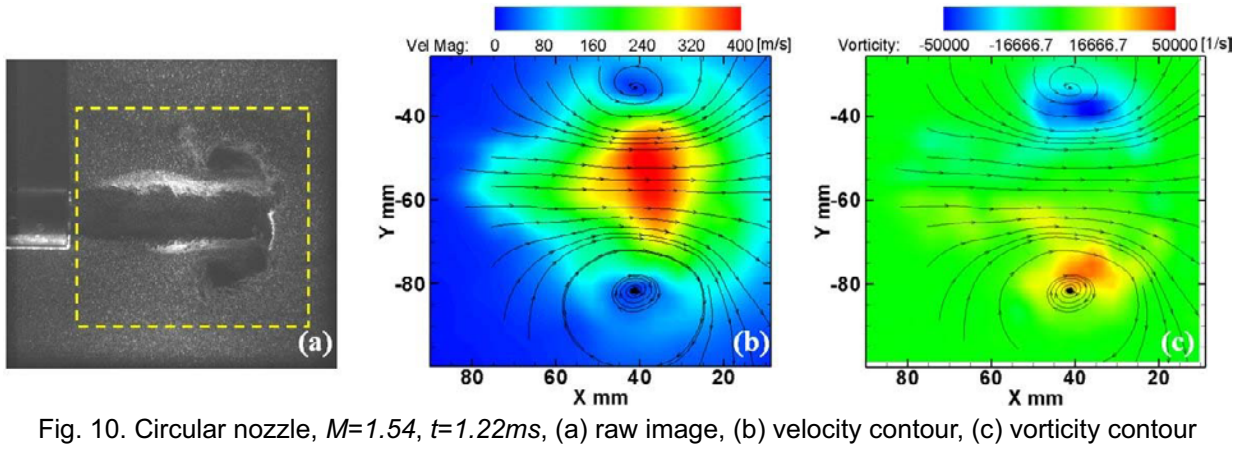

Fig. 10. Circular nozzle, *M=1.54*, *t=1.22ms*, (a) raw image, (b) velocity contour, (c) vorticity contour

10 depict these characteristics at two different times. From the series of images in Fig. 9 we can see that the almost triangular shaped core of the initially circular vortex loop rotates while maintaining its shape. The streamlines show a great tendency in entraining fluid ahead of the main structure into the circulatory motion of the cores. In Fig. 10, the initial triangular cores have become parallel to the direction of the flow and the magnitude of the velocity between the main cores and also the vorticity increases. The same behavior was also noted for $M= 1.66$.

4. Conclusions

The present study has presented global quantitative (PIV) maps of the velocity and vorticity fields as well as the flow streamlines generated by compressible vortex loops of various geometries. These include a square vortex loop with sides of *30×30mm*, two elliptical vortex loops with minor to major axes ratios of *0.4* and *0.6*, and finally a small circular vortex loop with an internal diameter of *15mm*, studied at Mach numbers of $M=1.54$ and *1.66*.

A secondary coaxial vortex loop with opposite circulation has been observed to form ahead of the primary loop. This secondary vortex loop formed at both Mach numbers. The deceleration of the flow ahead of the shock wave present within the primary vortex loop leads to the generation of a shear layer. As a result of Kelvin-Helmholtz instabilities a counter-rotating vortex forms at the apex of the primary vortex loop.

A new feature which, as the authors are aware has not been reported so far, is the formation of a third stronger vortex loop ahead of the primary one at higher Mach numbers for the elliptical and circular nozzles. The third vortex loop has circulation in the same direction as the primary loop, suggesting that perhaps it is formed by an impulsive behavior of the flow similar to the generation of the primary vortex loop. In the cases where the third vortex loop was observed, such as the elliptical nozzle *0.4* at $M=1.54$, an increase in the flow velocity was noticed in the velocity contours behind the third vortex loop. This increase in velocity could be due to the flow exiting the tube or to the non-uniform circulatory motion of the primary vortex loop. This creates velocities between the two cores which are higher at some instances and lower at others.

Acknowledgements

The authors would like to thank the technical and administrative staff at the University of Manchester and Mr. Parham Momeni and Mr. Ashiq Khalid for their help in the preparation and presentation of the manuscript. The technical assistance of Dr. Martin Hyde (*TSI*) for the installation and setup of the PIV system is also greatly acknowledged.

References

Arakeri, J. H., Das, D., Krothapalli, A. and Lourenco, L., Vortex ring formation at the open end of a shock tube: A particle image velocimetry study, Physics of Fluids, 16 (2004), 1008-1019.

Brouillette, M. and Hebert, C., Propagation and interaction of shock-generated vortices, Fluid Dynamics Research, 21 (1997), 159-169.

Dhanak, M. R. and DeBernardinis, B., The evolution of an elliptic vortex ring, J. Fluid Mech., 109 (1981), 189-216.

Grinstein, F. F. and DeVore, C. R., Dynamics of coherent structures and transition to turbulence in free square jets, Physics of Fluids, 8 (1996), 1237-1251.

Gutmark, E. J. and Grinstein, F. F., Flow control with noncircular jets, Ann. Rev. Fluid Mech., 3 (1999), 239-272.

Kontis, K., An, R., Zare-Behtash, H. and Kounadis, D., Head-on collision of shock wave induces vortices with solid and perforated walls, Physics of Fluids, 20 (2008).

Kontis, K., An, R. and Edwards, J. A., Compressible vortex-ring interaction studies with a number of generic body configurations, AIAA Journal, 44 (2006), 2962-2978.

Oshima, Y., Izitsu, N., Oshima, K. and Hussain, A. K. M. F., Bifurcation of an elliptic vortex ring, Fluid Dynamics Research, 3 (1988), 133-139.

Raffel, M., Willert, C. E. and Kompenhams, J., Particle Image Velocimetry, (1998), Springer.

Yoon, J. H. and Lee, S. J., Investigation of the near-field structure of an elliptic jet using stereoscopic particle image velocimetry, Meas. Sci. Tech., 14 (2003), 2034-2046.

Author Profile

Hossein Zare-Behtash: He received his BEng (Hons) in Aerospace Engineering in 2005 from the University of Manchester Institute of Science and Technology (UMIST) in the UK, and is currently a final year PhD student at the University of Manchester. His current research interests are Pressure-Sensitive Paints (PSP), experimental studies on compressible vortex loops using high-speed photography, schlieren (color / black and white), shadowgraphy, PIV and PSP techniques.

Nalleli Gongora-Orozco . She recived her BEng in Mechanical Engineering in 2002 from the Metropolitan Autonomous University in Mexico. She obtained her MSc degree in Theoretical and Applied Fluid Dynamics from the
University of Manchester in 2005. Currently she is studying internal shock wave interactions as part of her PhD in Aerospace Engineering at the University of Manchester.

Konstantinos Kontis: He is a Reader of Fluid Dynamics and Ground Testing Technology, and the Head of the Aerospace Research Group and Aero-Physics Laboratory at the University of Manchester, School of MACE, UK. He received his BEng (Hons) in Aeronautics, University of Bristol, UK (1993), and MSc and PhD in Aerodynamics, College of Aeronautics, Cranfield University, UK (1994, 1997). He is Chartered Engineer (2000), Hellenic Technical Chamber, Greece, and Eur.Ing. (2006), FEANI, Brussels, Belgium. He is Executive Member of the International Shock Wave Institute (2007) and member of the International Advisory Committee of ISSW. His present interests include: fundamental studies on incompressible and compressible flow structures and interactions, flow control of subsonic, transonic and hypersonic flows, development of optical imaging systems for aerospace applications, and interdisciplinary shock wave related phenomena and interactions.